AFRL-AFOSR-UK-TR-2016-0004

Growth of highly c-axis oriented and/or epitaxial single-domain b-axis oriented La5Ca9Cu24O41 thin films by pulsed laser deposition

Ioannis Giapintzakis
UNIVERSITY OF CYPRUS

04/01/2016
Final Report

Air Force Research Laboratory
AF Office Of Scientific Research (AFOSR)/ IOE
Arlington, Virginia 22203
Air Force Materiel Command

REPORT DOCUMENTATION PAGE

Form Approved
OMB No. 0704-0188

1. REPORT DATE *(DD-MM-YYYY)*	**2. REPORT TYPE**	**3. DATES COVERED** *(From - To)*
12/21/2015	Final	30-Sep-2014 to 29-Sep-2015

4. TITLE AND SUBTITLE
Growth of highly c-axis oriented and/or epitaxial single-domain b-axis oriented La5Ca9Cu24O41 thin films by pulsed laser deposition

5a. CONTRACT NUMBER
FA9550-14-1-0310

5b. GRANT NUMBER
Grant 14IOE086

5c. PROGRAM ELEMENT NUMBER
61102F

6. AUTHOR(S)
Giapintzakis, Ioannis

5d. PROJECT NUMBER

5e. TASK NUMBER

5f. WORK UNIT NUMBER

7. PERFORMING ORGANIZATION NAME(S) AND ADDRESS(ES)
UNIVERSITY OF CYPRUS, KALLIPLEOS 75, NICOSIA, , 1678, CY

8. PERFORMING ORGANIZATION REPORT NUMBER

9. SPONSORING/MONITORING AGENCY NAME(S) AND ADDRESS(ES)
EOARD
Unit 4515
APO AE 09421-4515

10. SPONSOR/MONITOR'S ACRONYM(S)
AFRL/AFOSR/IOE (EOARD)

11. SPONSOR/MONITOR'S REPORT NUMBER(S)
AFRL-AFOSR-UK-TR-2015-XXXX

12. DISTRIBUTION/AVAILABILITY STATEMENT
Distribution A: Approved for public release; distribution is unlimited.

13. SUPPLEMENTARY NOTES

14. ABSTRACT
This project attempted to grow La5Ca9Cu24O41 (LCCO) films on important substrates with the high-thermal-conductivity direction parallel or perpendicular to the surface of the substrate, counting success as demonstration of b-axis or c-axis oriented LCCO films along with measurement of bulk thermal conductivity. We succeeded in b-axis, but all efforts concerning growth of c-axis oriented films were unsuccessful. We extensively studied the influence of pulsed laser deposition growth parameters, trying various substrates or trying substrates with a buffer layer, but were not able to investigate substrates covered with carbon nanotubes as nanostructures with the desired dimensions proved unobtainable.

15. SUBJECT TERMS
EOARD, pulsed laser deposition, LCCO, La5Ca9Cu24O41, thermal conductivity, epitaxy

16. SECURITY CLASSIFICATION OF:			**17. LIMITATION OF ABSTRACT**	**18. NUMBER OF PAGES**	**19a. NAME OF RESPONSIBLE PERSON**
a. REPORT	**b. ABSTRACT**	**c. THIS PAGE**			PUTZ, VICTOR
					19b. TELEPHONE NUMBER *(Include area code)*
Unclas	Unclas	Unclas	SAR	24	235-6013

INSTRUCTIONS FOR COMPLETING SF 298

1. REPORT DATE. Full publication date, including day, month, if available. Must cite at least the year and be Year 2000 compliant, e.g. 30-06-1998; xx-06-1998; xx-xx-1998.

2. REPORT TYPE. State the type of report, such as final, technical, interim, memorandum, master's thesis, progress, quarterly, research, special, group study, etc.

3. DATE COVERED. Indicate the time during which the work was performed and the report was written, e.g., Jun 1997 - Jun 1998; 1-10 Jun 1996; May - Nov 1998; Nov 1998.

4. TITLE. Enter title and subtitle with volume number and part number, if applicable. On classified documents, enter the title classification in parentheses.

5a. CONTRACT NUMBER. Enter all contract numbers as they appear in the report, e.g. F33315-86-C-5169.

5b. GRANT NUMBER. Enter all grant numbers as they appear in the report. e.g. AFOSR-82-1234.

5c. PROGRAM ELEMENT NUMBER. Enter all program element numbers as they appear in the report, e.g. 61101A.

5e. TASK NUMBER. Enter all task numbers as they appear in the report, e.g. 05; RF0330201; T4112.

5f. WORK UNIT NUMBER. Enter all work unit numbers as they appear in the report, e.g. 001; AFAPL30480105.

6. AUTHOR(S). Enter name(s) of person(s) responsible for writing the report, performing the research, or credited with the content of the report. The form of entry is the last name, first name, middle initial, and additional qualifiers separated by commas, e.g. Smith, Richard, J, Jr.

7. PERFORMING ORGANIZATION NAME(S) AND ADDRESS(ES). Self-explanatory.

8. PERFORMING ORGANIZATION REPORT NUMBER. Enter all unique alphanumeric report numbers assigned by the performing organization, e.g. BRL-1234; AFWL-TR-85-4017-Vol-21-PT-2.

9. SPONSORING/MONITORING AGENCY NAME(S) AND ADDRESS(ES). Enter the name and address of the organization(s) financially responsible for and monitoring the work.

10. SPONSOR/MONITOR'S ACRONYM(S). Enter, if available, e.g. BRL, ARDEC, NADC.

11. SPONSOR/MONITOR'S REPORT NUMBER(S). Enter report number as assigned by the sponsoring/ monitoring agency, if available, e.g. BRL-TR-829; -215.

12. DISTRIBUTION/AVAILABILITY STATEMENT. Use agency-mandated availability statements to indicate the public availability or distribution limitations of the report. If additional limitations/ restrictions or special markings are indicated, follow agency authorization procedures, e.g. RD/FRD, PROPIN, ITAR, etc. Include copyright information.

13. SUPPLEMENTARY NOTES. Enter information not included elsewhere such as: prepared in cooperation with; translation of; report supersedes; old edition number, etc.

14. ABSTRACT. A brief (approximately 200 words) factual summary of the most significant information.

15. SUBJECT TERMS. Key words or phrases identifying major concepts in the report.

16. SECURITY CLASSIFICATION. Enter security classification in accordance with security classification regulations, e.g. U, C, S, etc. If this form contains classified information, stamp classification level on the top and bottom of this page.

17. LIMITATION OF ABSTRACT. This block must be completed to assign a distribution limitation to the abstract. Enter UU (Unclassified Unlimited) or SAR (Same as Report). An entry in this block is necessary if the abstract is to be limited.

FINAL TECHNICAL REPORT

CONTRACT No.: FA9550-14-1-0310

PROJECT TITLE: **Growth of highly *c*-axis oriented and/or epitaxial single-domain *b*-axis oriented $La_5Ca_9Cu_{24}O_{41}$ thin films by pulsed laser deposition**

PI: Ioannis (John) Giapintzakis

AFFILIATION: Nanotechnology Research Center &
Department of Mechanical & Manufacturing Engineering
University of Cyprus, Nicosia, Cyprus

DATE: December 21, 2015

Summary

The objective of this project was to grow highly-oriented epitaxial $La_5Ca_9Cu_{24}O_{41}$ (LCCO) thin films on technologically important substrates with the high-thermal-conductivity direction parallel and/or perpendicular to the surface of the substrate used. A successful project outcome was defined to be the demonstration of epitaxial single-domain *b-axis* oriented and/or highly *c-axis* oriented LCCO thin films along with the measurement of bulk-like thermal conductivity values for the obtained LCCO thin films. We have succeeded in obtaining epitaxial single-domain *b-axis* LCCO films on (1 1 0) SrTiO3 substrates with bulk-like thermal conductivity values along the cross-plane (*b-axis*) direction (~1 W/m-K). All efforts concerning the growth of epitaxial *c-axis* oriented LCCO films were unsuccessful. Within the elaboration of the project, issues such as the growth mode and the response of LCCO films under strain, were considered. To this end, we extensively studied the influence of the pulsed laser deposition (PLD) growth parameters; substrate nature, crystallographic orientation and surface termination; film thickness; and deposition geometry. Specifically, for Task 1 we deposited LCCO thin films with various thicknesses on (1 0 0) $SrTiO_3$, (1 1 0) $SrTiO_3$ and (1 0 0) $SrLaAlO_4$ flat surface substrates. We focused on the influence of the strain nature on the domain multiplicity of the grown films. Single-domain LCCO films based on HRXRD and HRTEM studies were obtained on (1 1 0) $SrTiO_3$ under certain conditions of growth temperature and film thickness. In addition, we investigated the influence of the miscut angle on the films' microstructure in the case of (1 1 0) and (1 0 0) $SrTiO_3$. In all cases the films were surprisingly randomly-oriented. For Task 2, we deposited LCCO films on different substrates either covered with a buffer layer of a-axis oriented $YBa_2Cu_3O_7$ (YBCO) or with a high-miscut surface. In all cases the obtained LCCO films were *b-axis* oriented. It is noted that the *a-axis* oriented YBCO films were grown directly on (1 0 0) $LaAlO_3$ substrates. Finally, the proposed third option of using substrates covered with carbon nanotubes was not investigated as we were not able to obtain nanostructures with the desired geometrical dimensions.

Task1: Growth of single-domain b-axis oriented LCCO films

Within the study of complex oxides significant attention has been paid on exploiting epitaxy to stabilize the oxide materials as thin films. Epitaxy, by definition, is used to describe the growth of a crystalline material on the surface of another with similar lattice structure/parameters. Between these two materials exists a quantifiable mismatch relationship:

$$\gamma(\%) = \frac{a_s - af}{a_f} * 100 \quad (1)$$

where a_f and a_s are the lengths of the crystal unit cell for the film and substrate, respectively. The multitude of deposited materials and choice of appropriate substrates result in unique sets of stresses and associated strains developed at the film-substrate interface. Stress represents the amount of force applied to a surface area, and strain (Ɛ) is the amount of (dimensionless) deformation that a material undergoes due to the stress, which is defined as:

$$\text{Ɛ}(\%) = \frac{dl}{l_0} * 100 \quad (2)$$

where d_l is the change in length and l_0 is the initial length.

Our initial experiments were focused on the effects of thermally induced Ɛ on the microstructure and stoichiometry of LCCO films grown on (1 1 0) $SrTiO_3$. By comparing the matching of the LCCO lattice parameters with the ones of $SrTiO_3$ (STO) and $SrLaAlO_4$ (SLAO), we determined that the best substrate choice for achieving our goal, i.e., *single-domain b-axis oriented LCCO films*, is the (1 1 0) oriented STO. In Table 1, a comparison of their bulk (strain free) lattice parameters indicates that in this case their matching is satisfactory but still not ideal, i.e., while there is a perfect matching for the adaptation of the LCCO *c-axis* along both in-plane crystallographic directions of the STO substrate ([1-10] or [001]), there is a considerable mismatch for the LCCO *a-axis* lattice parameter. By increasing the substrate temperature used during the growth of the LCCO films, our studies were intended to investigate whether the thermal expansion of the STO lattice has any influence on the films growth mode, in particular on their single-crystal-like character (domain multiplicity). The latter one is known to be sensitive to the films strained nature. Assuming that the only way Ɛ can be induced in a hetero-epitaxial film is by lattice matching with the substrate crystal, it is to be expected that an increase in the substrate temperature will lead to a thermal expansion of the substrate lattice and further induce variations to the film-substrate lattice matching, and thus to the film's strained nature. Figure 1a shows the expansion of the STO lattice, while Fig. 1b illustrates the expected amount

of Ɛ developed along the direction of *a*- and *c-axis* lattice parameters of the LCCO layers as a function of deposition temperature. Ɛ has been calculated based on the epitaxial relationships obtained from the in-plane XRD patterns (vide infra). We note that the Ɛ values presented in Fig. 1b are estimates, and have been calculated using the same room-temperature bulk parameters for all temperatures. A precise estimation of the Ɛ requires values for the thermal expansion coefficients (α), and their anisotropy depending on the particular case, of LCCO and STO. Unfortunately, α_{LCCO} is not known. Also, the calculations are based on (i) the validity of one of the most fundamental assumptions about pulsed laser deposition, that this technique has an exquisite ability to maintain stoichiometric transfer of components from target to film, and (ii) the assumption of a "*defect free growth process*", hence, it excludes the existence of any factor which may favor Ɛ relief, i.e., point defects, coalesce of the grains, surface cracks, etc.

Table 1 *The mismatching of the LCCO lattice constants with the in-plane directions of the (110) STO and (100) SLAO substrates. The presented values have been calculated using: a=11.301 Å, b=12.612 Å, c=27.602 Å (according to # ICDD 01-084-1761, space group Cccm (86)) for the LCCO compound; a=b=c=3.905 Å for STO (according to # ICDD 00-635-0734, space group Pm-3m (221)); and a=b=3.756 Å, c=12.635 Å (according to # ICDD 00-045-0637, space group I4-2m (136)) for SLAO.*

Substrate	In-plane direction	γ (%)		
		a_{LCCO}	b_{LCCO}	c_{LCCO}
(1 1 0) $SrTiO_3$	[1 - 1 0]	-2.26	-12.42	0.03
	[0 0 1]	3.66	-7.11	-0.96
(1 0 0) $SrLaAlO_4$	[0 1 0]	11.80	-10.65	-4.74
	[0 0 1]	-0.29	0.18	-8.44

For the calculation of the expected Ɛ we have used the following equations:

$$\varepsilon_{a-axis} = \frac{3*a_{STO}^{Ts} - a_{LCCO}^{bulk}}{a_{LCCO}^{bulk}} \quad (3)$$

$$\varepsilon_{c-axis} = \frac{5*\sqrt{2*(a_{STO}^{TS})^2} - c_{LCCO}^{bulk}}{c_{LCCO}^{bulk}} \quad (4)$$

where a_{STO}^{Ts} represents the value of the STO *a-axis* lattice parameter at the temperature where the deposition has been made, and a, c_{LCCO}^{bulk} the bulk values of the LCCO *a-* and *c-axis* lattice parameters.

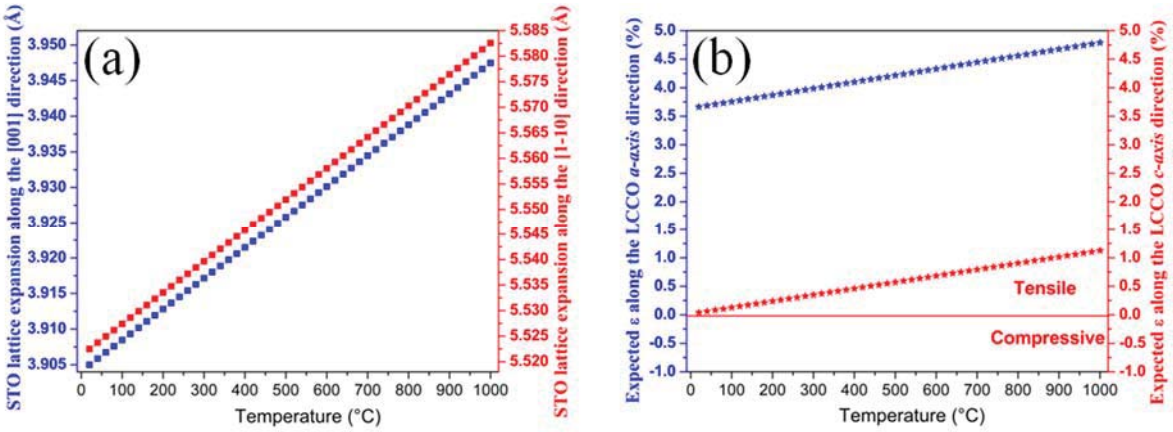

Figure 1 (a) *Extrapolated thermal expansion of the STO lattice along both in-plane directions (α_{STO}=11.1x $10^{-6}°C^{-1}$), and* ***(b)*** *calculated ε evolution over temperature.*

Figure 2a shows the X-ray diffraction (XRD) patterns of LCCO films grown on (1 1 0) STO in the temperature range of 500-700°C, with steps of 40°C. This temperature range was chosen based on prior studies which have shown that for deposition temperatures below 500°C the films exhibit poor crystallinity, while above 750°C secondary phases appear. The films have been grown using an average laser fluence (Φ) of ~ 1.3 J/cm^2, at a repetition rate (RR) of 1 Hz, and a target-to-substrate separation distance of 4.5 cm. During the deposition process the oxygen pressure in the chamber was kept constant at 1 mbar, and the same number of laser pulses (250) was applied for the growth of all films resulting in the growth of 60 nm-thick LCCO layers (deposition rate of 2.2 Å / laser pulse). The XRD patterns revealed that together with the substrate's (h h 0) peaks, the (0 k 0) reflections of LCCO structure were only observed in the entire scanned range up to 2θ=90^o. The absence of other diffraction peaks implies that the films are highly textured along the *b-axis* (the Cu-O ladders and chains are parallel to the substrate surface). As Fig. 2b indicates the *b-axis* lattice parameter, calculated form the position of the (0 8 0) LCCO diffraction peak, exhibits an increase over deposition temperature with a lattice enlargement along this direction of 0.05 Å (3 %). Surprisingly, for all deposition temperatures its

length was larger than the relaxed bulk value, indicating the presence of a tensile Ɛ perpendicular to the substrate surface.

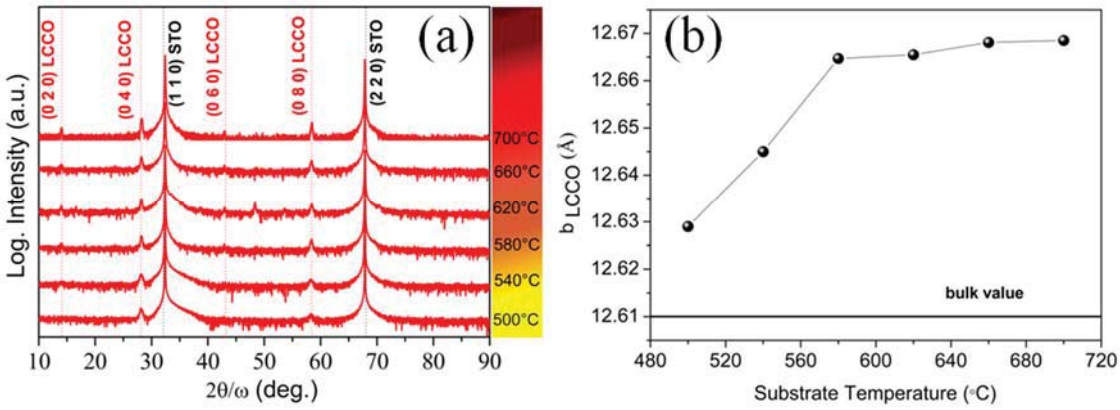

Figure 2 (a) *XRD patterns of LCCO films grown on (1 1 0) STO at different deposition temperatures, and* ***(b)*** *the evolution of b-axis lattice parameter over deposition temperature.*

The substrate-film epitaxial relationships were determined by performing azimuth (φ) -scans on skew planes of the film and the substrate. For the STO substrate we used the {1-1 0} and {0 0 2} skew planes, whereas for the LCCO film the {6 0 0} and {0 0 20}. In case of a single-domain *b-axis* oriented LCCO film, two peaks set at 180° should diffract in a φ-scan over a complete circle, for both, the orthorhombic LCCO film as well as for the tetragonal symmetry of the (1 1 0) oriented STO substrate. Indeed, two peaks arranged in a two-fold symmetry can be observed in Fig. 3a, confirming the single-crystal-like character of the films. The coincidence of the film's (0 0 20) azimuth with the (1 -1 0) of the substrate, and (6 0 0) $_{LCCO}$ with (0 0 2) $_{STO}$ indicates that the in-plane orientation is such that LCCO [0 0 1] ‖ STO[1 -1 0] and LCCO [1 0 0] ‖ STO [0 0 1]. The growth mode is, therefore, driven by the close matching of the LCCO *c-axis* on the [1 -1 0] direction of STO substrate, see Table 1. The aforementioned epitaxial relationships have also been confirmed by transmission electron microscopy (TEM). The bright field image of an LCCO film grown at 700°C is shown in Fig. 3b. Its thickness varies from 45 up to 60 nm and consists of columnar crystals, 20-80 nm in width. The majority of these crystals grow epitaxially on the substrate with [0 1 0] LCCO ‖ [1 1 0] STO, while in several cases *b-axis* is slightly off this orientation. In the high resolution image of Fig. 3c the interface between film and substrate is given at the base of three adjacent crystals. The growth of the film starts directly

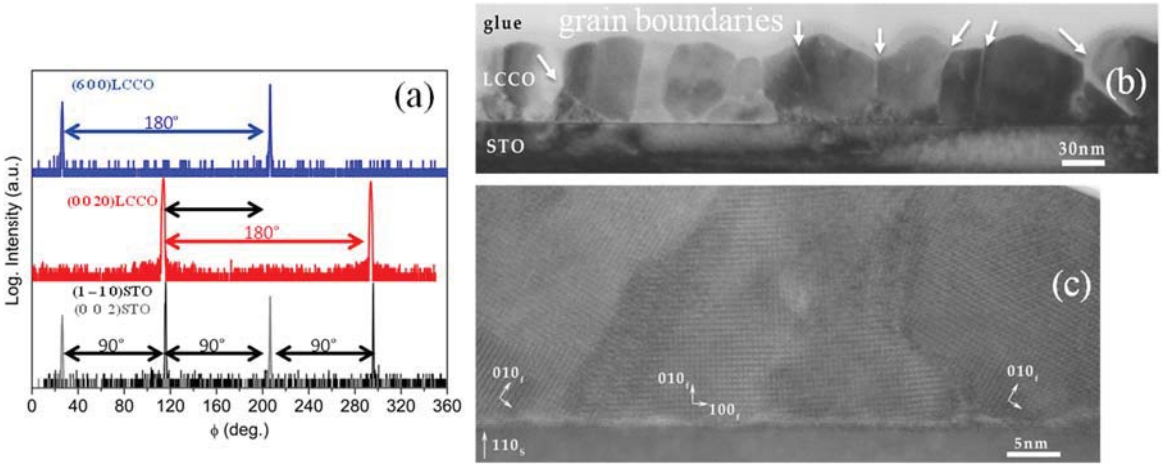

*Figure **3 (a)** φ-scans obtained for an LCCO film grown on (1 1 0) STO at 700°C using 250 laser pulses, **(b)** bright field cross-section TEM image, and **(c)** high resolution cross-section TEM image.*

on the substrate and no amorphous layer is observed. However, some other imperfections of the growth mode are observed (shown by arrows in Fig. 3b).

From the position of the (6 0 0) and (0 0 20) LCCO diffraction peaks, see Fig. 4a, we calculated the values of the *a-* and *c-axis* lattice parameters. As Fig. 4c shows, the *a-axis* lattice parameter exhibits a nearly linear decrease as a function of deposition temperature, and the obtained values indicate the presence of a tensile type of Ɛ (parallel to the substrate surface), similar to the one observed in the out-of-plane (*b-axis*) direction. On the other hand, along the other in-plane direction the increase of deposition temperature does not seem to affect the LCCO lattice, since the obtained *c-axis* values are very close to the bulk one and nearly the same for all temperatures. It is important to note that for all temperatures the *c-axis* length is smaller than the bulk value, suggesting that along this in-plane direction the film's Ɛ nature has been changed from tensile (*a-axis*) to compressive. Based on the experimentally obtained lattice parameters, Fig. 4d illustrates the evolution over deposition temperature of the Ɛ developed in the LCCO layer along both in-plane directions, as well as the residual one in the out-of-plane direction. The highest Ɛ values were observed along the *a-axis* direction, ranging from 0.6-1.7%, with a linear decrease over deposition temperature. As a result of the *a-axis* expansion, an in-plane compressive Ɛ is developed along the other in-plane direction (*c-axis*) which leads to an elongation along the normal direction (*b-axis*). These observations are rather surprising considering that: *i)* from the calculated Ɛ evolution, see Fig. 1b, we expected a linear expansion

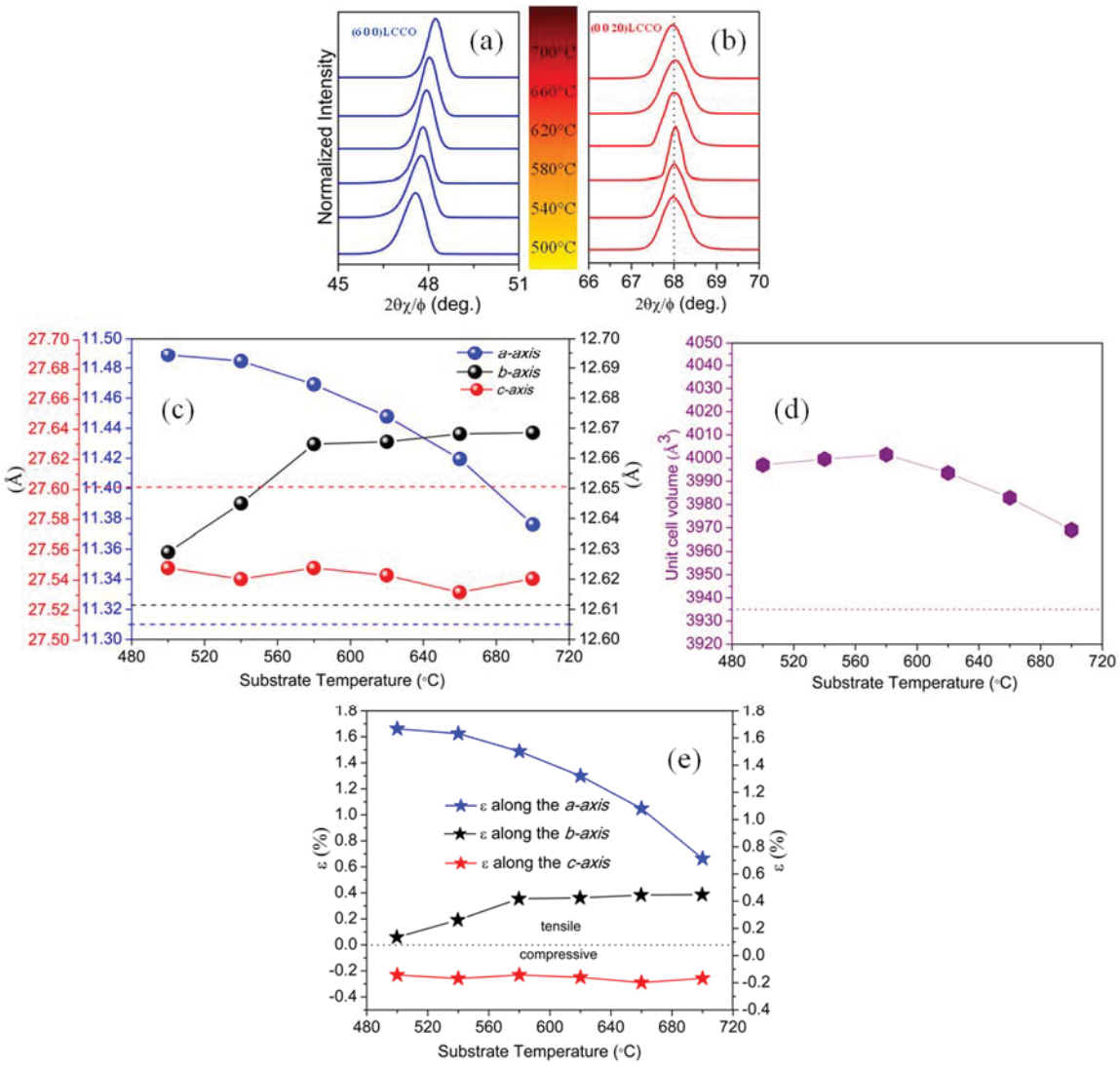

Figure 4 *Detailed 2θχ/φ-scans around* ***(a)*** *the LCCO (6 0 0), and* ***(b)*** *LCCO (0 0 20) diffraction peaks,* ***(c)*** *LCCO lattice parameters vs. deposition temperature,* ***(d)*** *the in- and out-of-plane epitaxial Ɛ vs. deposition temperature, and* ***(e)*** *LCCO unit cell volume vs. deposition temperature. The dashed lines represent the bulk values of the LCCO unit cell.*

along both in-plane directions (enlargement of the *a-* and *c-axis* lattice parameters) as the deposition temperature in increased, and as a result of the unit cell tendency to preserve its volume (Poisson effect) a contraction in the out-of-plane direction (*b-axis*), and *ii)* under epitaxial growth conditions the in- and out-of-plane Ɛ normally cancel each other having opposite signs (see Ɛ along the *a-axis vs.* Ɛ along the *b-axis*). There are several scenarios which may support such behavior. First, if within this temperature range the thermal expansion coefficient of LCCO is larger than the STO one then the LCCO *a-* and *c-axis* lattice parameters are actually larger than the template provided by the STO substrate, resulting in a contraction

along the in-plane directions, and, as a consequence, to a unit cell expansion in the out-of-plane direction (*b-axis* direction), as we have observed. However, this scenario does not explain the temperature evolution and the length of *a*- and *c-axis* lattice parameters. A second scenario has to do with the formation of O vacancies on the substrate surface upon the increase of the substrate temperature under reducing atmosphere. These O vacancies will lead to changes in the Ti valence (Sr is limited to a single oxidation state of 2+), and, more importantly, to repulsion between the positively charged Sr or Ti cations, hence, resulting in an expansion of the STO lattice. Such a scenario explains the observed enlargement along the LCCO *a-axis*, but not the one along the *b-axis* or the *c-axis* contraction. Nevertheless, the existence of such processes requires a powerful in-situ and, ideally, real-time characterization.

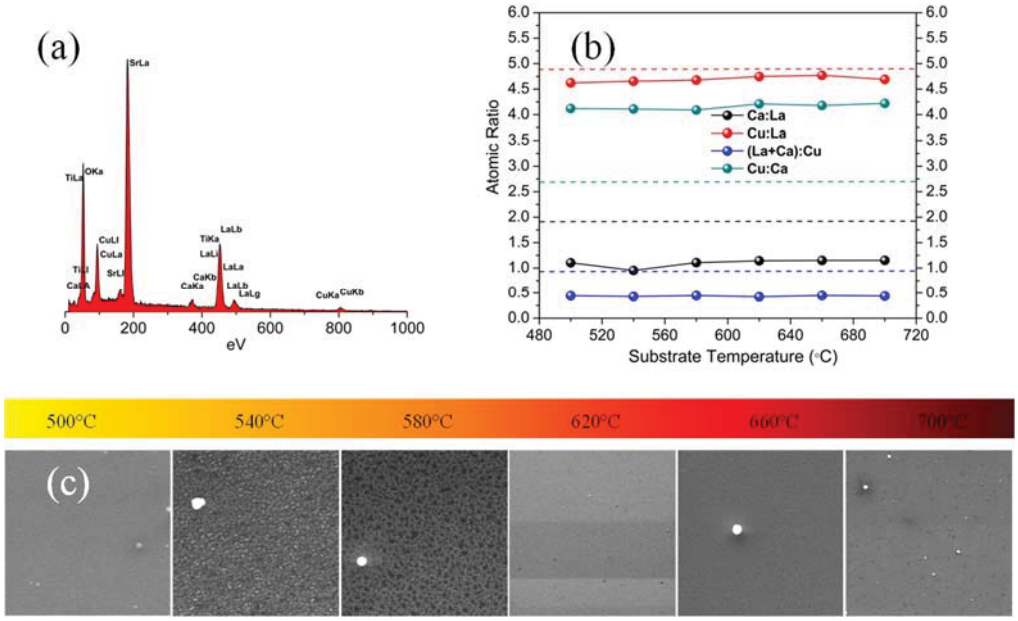

Figure 5(a) *Typical EDS spectrum obtained for an LCCO film grown on (1 1 0) STO,* ***(b)*** *elemental ratios vs. deposition temperature. The dashed lines represent the elemental ratios of bulk LCCO.* ***(c)*** *SEM micrographs of LCCO films deposited at different deposition temperatures.*

Energy dispersive X-ray spectroscopy (EDS) analysis verified the absence of impurities in the films composition and showed that in this range the substrate temperature does not affect their stoichiometry. As Fig. 5b shows, the films exhibit a uniform composition over temperature. However, the elemental ratios suggest that the films are slightly non-stoichiometric; there is a Ca-deficiency. The observed deficiency could be linked to the compressive Ɛ developed along the *c-axis*, as the Ca atoms are located along the *c-axis* direction, in between the Cu-O chains and

ladders (see Fig. 9) and also have the largest ionic radius among the constituent elements (176 pm, in comparison with 138.91 pm for La, 132 pm for Cu and 66 pm for O).

Concerning the films' topology, scanning electron micrographs (SEM) revealed that as the deposition temperature is increased the films become more granular, and the number and size of micron-scale particles present on the surface increases.

The second parameter we have investigated for the LCCO films grown on (1 1 0) STO was the maximum layer thickness for which the films preserve a single-domain structure. Based on the previously discussed structural characterization, the deposition temperature of 700°C was selected for this study (high peak intensity in the XRD pattern; see Fig. 2a). The film thickness was controlled by the number of laser pulses applied during the growth growth and it has been varied from 15 to 160 nm. The obtained results show that the envisaged single crystal character is preserved only for layer thicknesses up to ≈ 60 nm, i.e., films grown using 250 laser pulses or less. The experimental φ-scans obtained on films grown using more laser pulses have shown 8 diffraction peaks, set apart at 45° intervals. This could be explained by the existence of four in-plane orientation variants of LCCO set at 45° from each other, whose corresponding peaks are marked in the φ-scans from 1 to 4 in Fig. 6b.

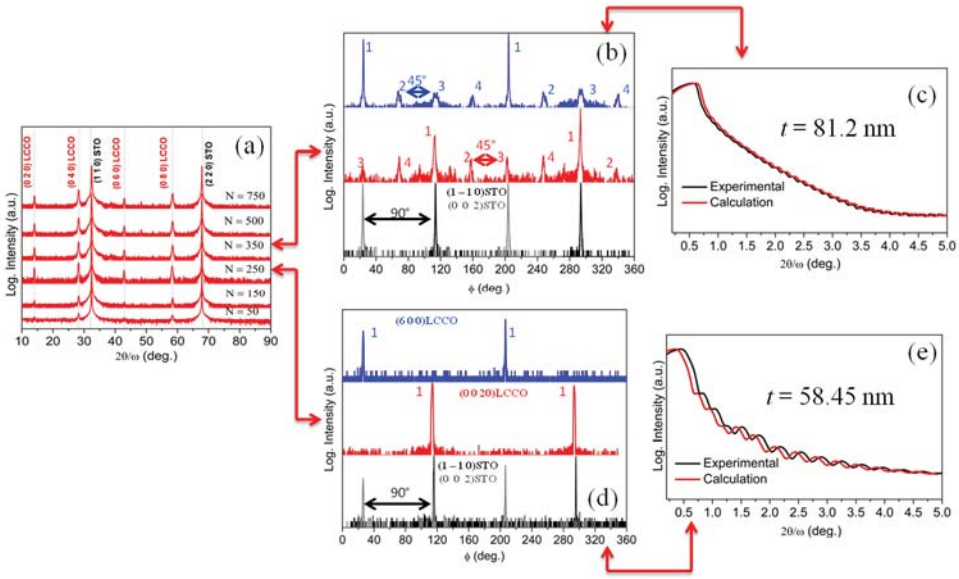

Figure 6 (a) *XRD patterns of LCCO films grown on (1 1 0) STO at 700°C using different number of laser pulses,* ***(b)*** *φ-scans obtained on the LCCO film grown at 700°C using 350 laser pulses (multiple domains),* ***(c)*** *X-ray reflectivity (XRR) profile of the film from Fig. 6b,* ***(d)*** *φ-scans on the LCCO film grown at 700°C using 250 laser pulses (single domain), and* ***(e)*** *XRR profile of the film presented in Fig. 6d.*

The intensity variation of these peaks suggest that the majority of the LCCO crystals are epitaxially grown with [0 0 1] LCCO ‖ STO [1 -1 0]; the high intensity peaks diffracted by the (0 0 20) LCCO diffraction planes (marked with 1 in Fig. 6b) have the same inclination as the (1 -1 0) planes of the substrate. This tendency of the LCCO *c-axis* to adapt parallel to the [1 -1 0] direction of the STO could be explained by the fact that along this direction the STO substrate provides the best lattice matching (see Table 1), as well as the same number of O ions, with a similar interatomic separation distance as the Cu cations along the LCCO *c-axis* (see Fig. 7c).

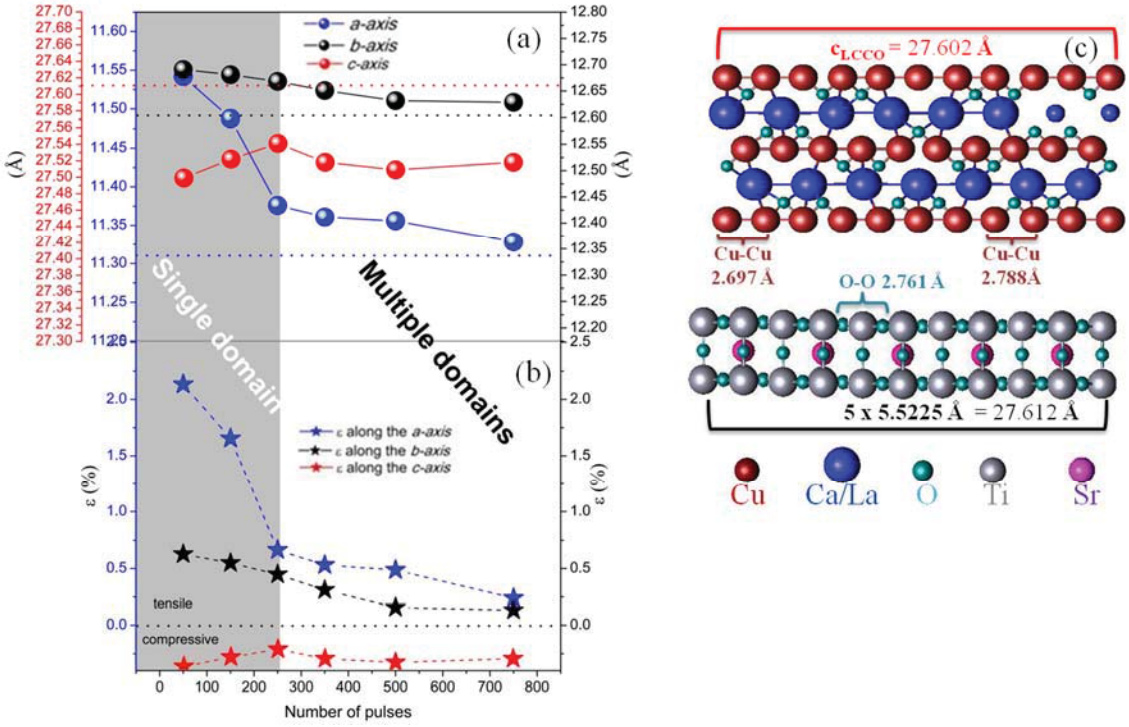

Figure 7 (a) *LCCO lattice parameters vs. number of pulses (layer thickness),* ***(b)*** *the in- and out-of-plane epitaxial Ɛ vs. layer thickness, and* ***(c)*** *schematic representation of the adaptation of LCCO c-axis ∥ to the [1 -1 0] direction of the STO substrate, consistent with the φ-scans.*

The single crystal character of the films has proven to be highly sensitive to the films strained nature as a reduction of only 0.1 % in the Ɛ retained in the LCCO layer along the *a-axis* is immediately accompanied by the formation of multiple domains (see Figs. 7b and 6b). We have associated the formation of multiple domains solely with the Ɛ developed along the *a-axis* based on the observation that the values obtained for *c-axis* exhibited negligible changes (0.02 Å, 0.1%) as function of layer thickness, indicating that the compressive Ɛ developed along this direction is constant; while the *a-axis* lattice parameter exhibits a linear decrease towards the bulk value by increasing the layer thickness, from 11.558 to 11.327 Å (2.3%) suggesting a

reduction in the tensile Ɛ developed along this direction. This Ɛ reduction by increasing the layer thickness could be attributed to one of the intrinsic problems of PLD, namely, the creation of nanoscale defects in thick films. Above a certain thickness, specific for each material and known as the pseudomorphism limit, a maximum storage capacity of elastic energy is reached. As a result, defects are created and/or changes of growth mode occur, leading to the minimization of epitaxial Ɛ developed in the early stages of the growth process. Typical defect formations are: stacking faults, low–angle grain boundaries, twining and misfit dislocations.

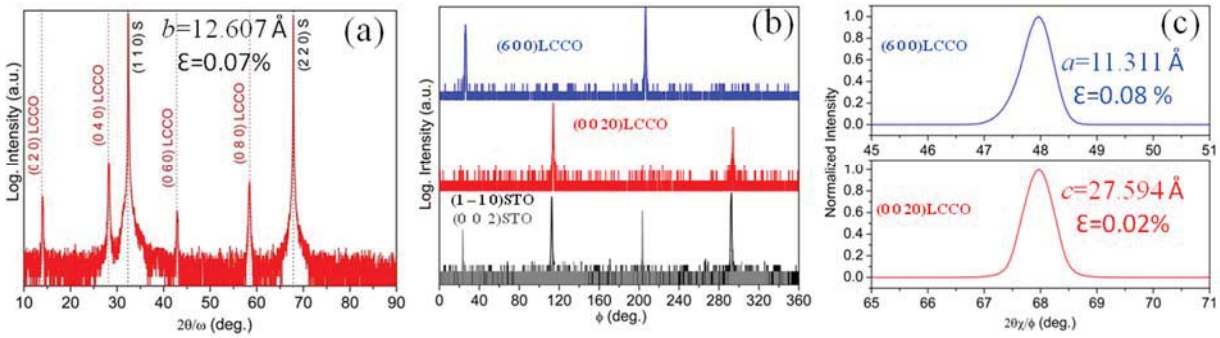

Figure 8 (a) *XRD pattern of an LCCO film grown on (1 1 0) STO at 500°C using 2500 laser pulses,* ***(b)*** *φ-scans on the same sample confirming its single crystal character, and* ***(c)*** *detailed 2θχ - φ scans around the (0 0 20) and (6 0 0) LCCO diffraction peaks. We note that the average internal Ɛ developed in such films is almost zero as the obtained lattice parameters are very close to the bulk ones, suggesting a linear increase in the number of defects with increasing layer thickness.*

We were, however, able to achieve the growth of single-domain films even for layer thicknesses of 450 nm by using a lower substrate temperature. Figure 8b shows the φ-scans obtained on a LCCO film grown using a deposition temperature of 500°C and 2500 laser pulses. The coincidence between the film's and the substrate's azimuths confirms the single-crystal-like character and points to the same epitaxial relationships as the ones obtained on the 60 nm-thick films grown at a deposition temperature of 700°C (see Figs 3a and 5d). The preservation of a single orientation variant above the thickness limit found in the case of films grown at 700°C may be attributed to the lower thermal energy. During the growth process, the arriving atoms (or molecules) diffuse some distance on the substrate surface at the cost of kinetic and thermal energy (the latter one being mainly provided by the substrate temperature), until a stable, energetically favorable bond with other film atoms or substrate atoms is established. Consequently, a lower substrate temperature could prevent the formation of multiple orientation variants by decreasing the distance across which the ablated atoms can diffuse.

The thermal conductivity (λ) of 450 nm-thick LCCO thin films grown on (1 1 0) STO at 500°C was measured using the time-domain thermoreflectance (TDTR) method. Based on prior studies performed on LCCO single crystals, the measurements were carried out at T=315 K (more details about the TDTR measurements in the Methods section), and for repeatability reasons it was decided to compare the values obtained on two films grown under the same conditions. The obtained results presented in Table 2 show that there is no anisotropy between the λ values measured along the *a*- and *c-axis*, suggesting only the existence of phononic thermal transport.

Table 2 *Values of the λ measured along the in- and out-of-plane directions on LCCO films grown on (1 1 0) STO at 500°C, using 2500 laser pulses.*

	NbV contact thickness (nm)	LCCO layer thickness (nm)	λ(W/m · K)		
			In-plane		Out-of-plane
			a-axis	*c-axis*	*b-axis*
Sample 1	67	450	1 ±0.4	1 ±0.4	0.8 ±0.05
Sample 2	70	450	1.2 ±0.3	1.2±0.3	0.8 ±0.05

We have attributed this result to the suppression of the magnon-contribution caused by the formation of grain boundaries between the epitaxially grown LCCO columnar crystals; it has been well established by detailed studies on single crystals that the two-peaks feature in *λ(T)* of LCCO is induced by two main contributions, one due to phonons responsible for the low-temperature peak, and the other peak at higher temperatures is related to itinerant spin excitations in the Cu-O-Cu ladders. The formation of these nano-scale grain boundaries (marked with arrows in Fig. 3b) most likely results in the break-up of the antiferromagnetic Cu-O-Cu bonds and, as a consequence, interrupts the magnetic excitations responsible for the additional high-temperature maximum. We underline that Cu-O-Cu chains and ladders are formed along the *c-axis* and are aligned parallel to the substrate surface (see Fig. 9). Also, other atomic-scale defects such as the observed Ca deficiency (see Fig. 5) could quench the antiferromagnetic order. Unfortunately, thinner films could not be measured due to the TDTR film thickness limitations (minimum layer thickness 300 nm).

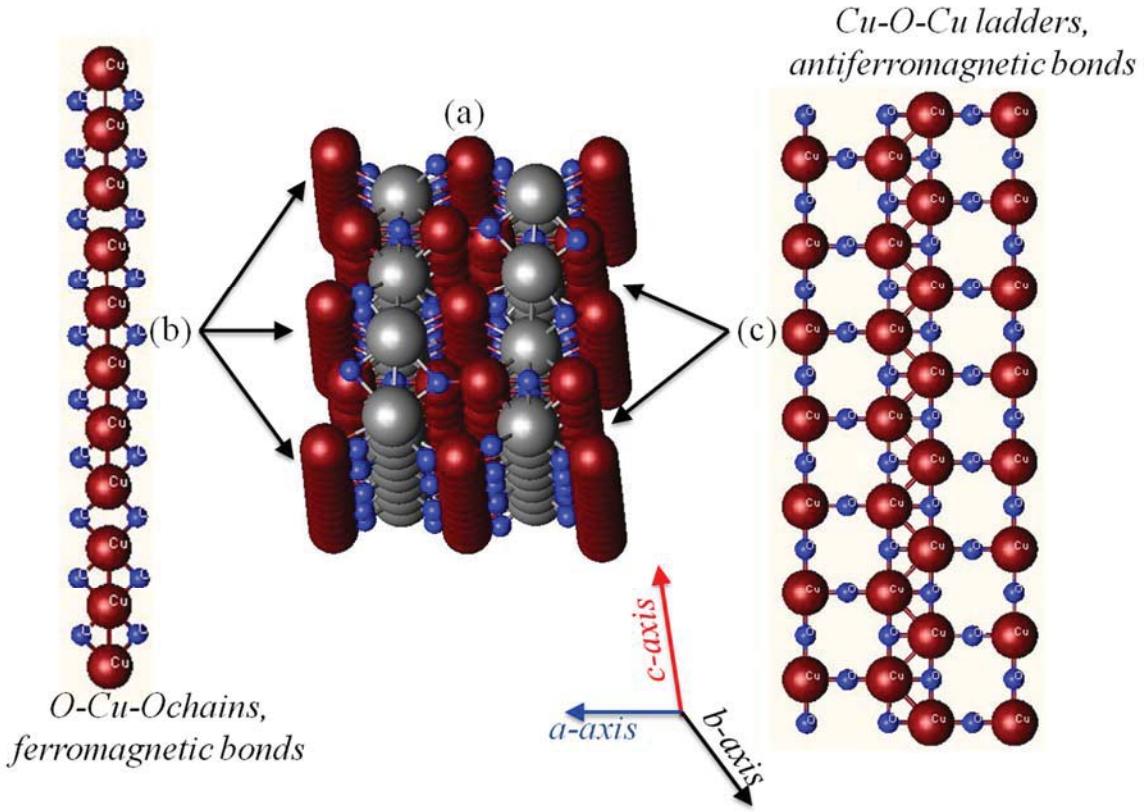

Figure 9 (a) *Crystal structure representation of the LCCO unit cell. The crystal structure consists of two interpenetrating subcells formed by the Cu_2O_3 and CuO_2 layers, and in between alternating La/Ca ions. The CuO_2 contains linear chain of Cu-ions, which are linked by a two nearly 90° O-Cu-O bonds, while in the other subcell the Cu_2O_3-ladder are linked by 180° Cu-O-Cu antiferromagnetic bonds. The layers in both subcells are stacked along the b-axis, whereas the one dimensional chains and the two leg ladders are aligned incommensurably along the c-axis with an average cell of 7 x c (ladder) and 10 x c (chain), respectively,* ***(b)*** *top view of the chains formed in the CuO_2 layers, and* ***(c)*** *top view of the ladders formed along the Cu_2O_3 planes direction.*

In our attempt to achieve the growth of thick single-domain *b-axis* oriented films, we have also used (1 0 0) STO and (1 0 0) SLAO substrates. Following the previously discussed influence of the layer thickness and deposition temperature on the films growth mode, it has been decided to carry out depositions at temperatures in the range of 500-700°C using the same number of laser pulses (250), and the rest of the deposition parameters held the same.

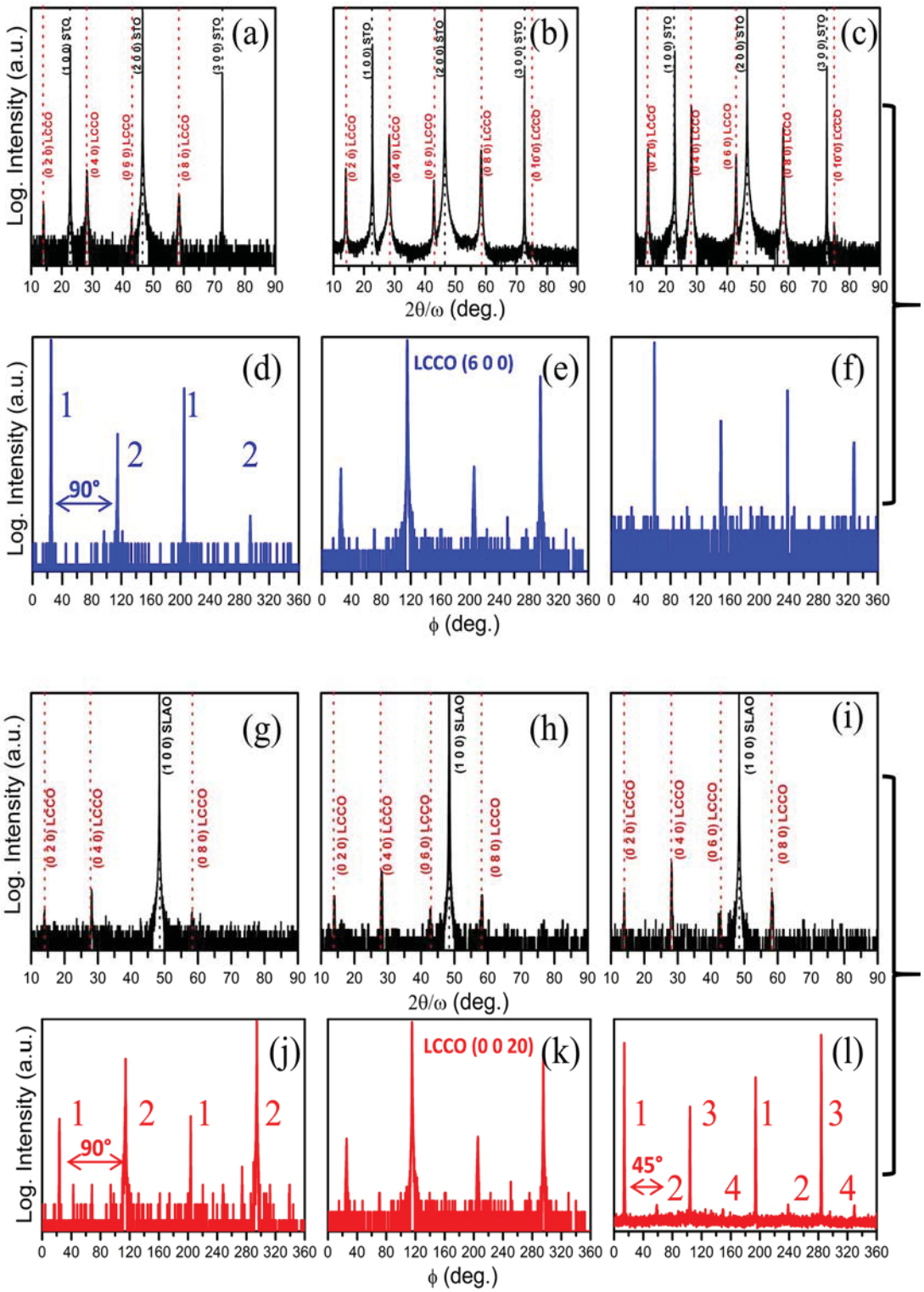

Figure 10 *XRD patterns of LCCO films grown on* ***(a)*** *(100) STO at 500°C,* ***(b)*** *(100) STO at 600°C,* ***(c)*** *(100) STO at 700°C,* ***(g)*** *(100) SLAO at 500°C,* ***(h)*** *(100) SLAO at 600°C,* ***(i)*** *(100) SLAO at 700°C, and their corresponding φ-scans in* ***(d, e, f)*** *and* ***(j, k, l),*** *respectively.*

Irrespectively of their lattice matching or growing temperature, the growth mode was dominated by the intrinsic tendency of LCCO films to adapt with the Cu-O chains and ladders parallel to the substrate surface. In both cases, the films were *b-axis* oriented and exhibited multiple domain variants. The adaptation of *b-axis* oriented films on the surface of (1 0 0) STO resulted in the formation of 2 orientation variants separated by 90°. The same tendency has been observed in the case of films grown on (1 0 0) SLAO at 500°C and 600°C, while the films grown using deposition temperatures ≥ 700°C resulted to the formation of 4 domain variants separated by 45°, see Figs 10g, h, i. Some of these results are quite surprising, considering that the out-of-plane *b-axis* lattice parameter of the LCCO film fits much better to that of the SLAO substrate (γ= 0.18%), than the in-plane *c-axis* lattice parameter (γ= 8.44%, see also Table 1) and, thus, in this case we expected the films to exhibit some degree of (h 0 l) texture.

Task 2: Growth of c-axis oriented LCCO films

As the results presented in the first part (Task 1) of this report demonstrate, the films growth mode is dictated by the tendency of the LCCO unit cell to adapt with the Cu-O chains and ladders parallel to any surface resulting in a texture along the *b-axis*, whereas their single-crystal-like character has proven to be sensitively limited by the films strained nature. As the ε is relieved (either by increasing the layer thickness as in the case of films grown on (110) STO, or due to the high lattice mismatch as in the case of films grown on (100) STO and (100) SLAO) the obtained LCCO films exhibited 2 or 4 domain variants depending on deposition temperature and substrate choice. Normally, only the lattice misfit between the substrate and the film is considered to govern the structure and, further, the physical properties of epitaxial thin films, and, in principle the lattice misfit strain energy can be partially/fully released only by the creation of defects, or through the formation of edge dislocations that periodically distribute along the interface. In our attempt to change the growth mode by preserving the ε retained in the films structure, we have additionally investigated the influence of the substrate miscut angle and the effect of the substrate surface-step-terraces formation on the epitaxial nature of the films. In this regard, we have used STO substrates with various miscut angles (α) along specific crystallographic directions (β), see Table 3.

Table 3 *Miscut angle values and directions of the STO substrates.*

Sample Code	Substrate orientation	Miscut direction	Miscut angle (°)
M1	(1 0 0)	[1 1 0]	8
M2	(1 0 0)	[1 1 0]	10
M3	(1 0 0)	[0 1 0]	8
M4	(1 0 0)	[0 1 0]	4.5
M5	(1 10)	[1 1 0]	3
M6	(1 10)	[0 0 1]	3

The XRD patterns presented in Fig. 12a show that for both STO orientations investigated, and independently of the substrate miscut, the films exhibited a preferred (h k 0) orientation. These observations are quite unusual since the LCCO films have hitherto showed an intrinsic tendency towards *b-axis* growth, including the growth on non-crystalline substrates such as α-SiO_2 (not shown here). We attributed this adaptation mode of the LCCO lattice to the undefined crystallographic termination of the last atomic plane throughout the surface of the as-received substrates. Also due to the high miscut angle, the inclination of the (1 0 0) / (1 1 0) atomic planes (the out-of-plane direction of the STO substrates) is not the same over the entire area of the substrate surface. An ideal surface similar with the one illustrated in Fig. 12c required further chemical etching followed by a thermal treatment. The initial chemical etching process was performed using a buffered (5%) hydrofluoric acid (BHF) solution, and it was applied in order to selectively remove the surface SrO_x. In order to facilitate the crystallization, and promote the formation of well-defined steps and terraces on the substrate surface (see Figs 11b, c, d, and e) a final annealing step was performed in O_2 flow for 2 h. We note that in the case of (1 1 0)-oriented STO substrates this procedure cannot be performed as the surface presents both TiO- and SrO-termination. After the growth of LCCO films on the surface of the treated substrates, the films orientation has switched from (h k 0) to a prevalent (0 k 0) one.

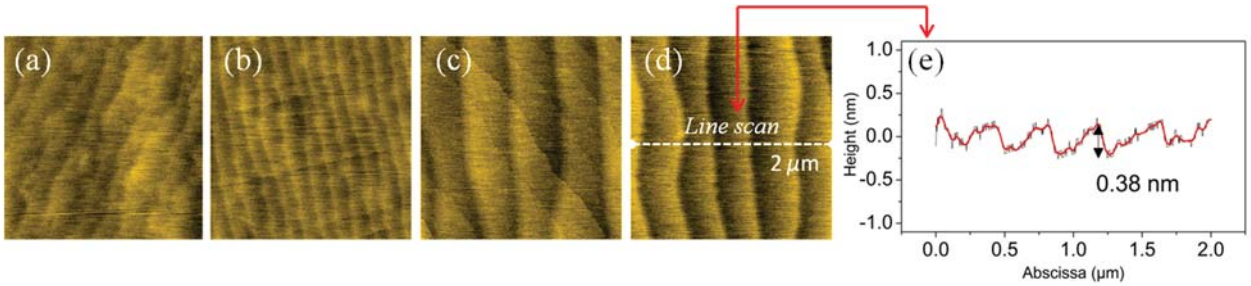

Figure 11 *Topographic AFM scan on the surface of* ***(a)*** *as-received STO substrate,* ***(b)*** *after been etched for 18s and annealed at 1000°C for 2h,* ***(c)*** *after been etched for 18s and annealed at 1000°C for 4h,* ***(d)*** *after been etched for 1m and annealed at 1000°C for 2h.* ***(e)*** *Line scan profile on the substrate form Fig. 11d indicating the formation of steps and terraces of atomic-scale.*

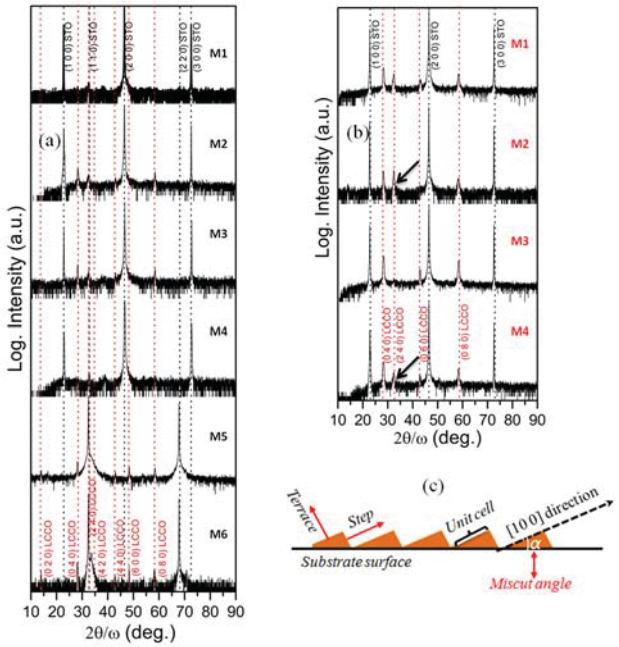

Figure ***12 (a)*** *XRD patterns of LCCO films grown on as-received miscuted STO substrates at 700°C and 250 laser pulses,* ***(b)*** *XRD patterns of LCCO films grown on miscuted STO substrates under the same conditions as Fig. 12a after the substrates have been etched for 1m and annealed at 1000°C for 2h, and* ***(c)*** *schematic depicting the morphology of an ideal substrate surface and the miscut angle. The miscut direction is defined by the projection of the surface normal on the out-of-plane substrate direction and the in-plane direction.*

The growth of *a-axis* oriented $YBa_2Cu_3O_7$ (YBCO) films has proven to be a challenging task since the obtained YBCO layers have shown a similar tendency as the LCCO ones, i.e., they grow with the Cu-O chains parallel to any depositing surface. Our studies included the growth

of YBCO films on different substrates which exhibit a better lattice matching with the *b*- and *c-axis* lattice parameters of YBCO than with *a-axis*, see Table 4.

Table 4 *The mismatching of the YBCO lattice constants with the in-plane directions of the used substrates.*

Substrate	In-plane direction	γ (%)		
		a_{YBCO}	b_{YBCO}	c_{YBCO}
(1 0 0) $SrTiO_3$	[0 01]	2.41	0.62	0.705
	[1 0 1]	-3.42	-5.12	-5.05
(1 0 0) MgO	[0 1 0]	10.59	8.66	8.75
	[1 0 1]	3.809	1.97	2.05
(1 0 0) $LaAlO_3$	[0 1 0]	-2.30	-0.57	-2.32
	[1 0 1]	-7.93	-6.24	-7.831

Following the current literature results the YBCO layers have been grown in an oxygen pressure (P_{O2}) of 0.2 mbar, and during the sample cooling the P_{O2} has been increased to 500 mbars. The XRD investigations on the obtained films have shown that the films grown on (1 0 0) STO and (1 0 0) MgO exhibit a preferred *c-axis* orientation independently of the used deposition parameters (e.g., Fig. 13a, b). We were, however, able to achieve the growth of *a-axis* oriented YBCO films on (1 0 0) $LaAlO_3$ (LAO) substrates. In this case, the films grown at deposition temperatures ≤ 630°C presented a preferred *a-axis* orientation, while for higher temperatures they become (h 0 l) oriented, see Figs 13 d and e. As Fig. 13f shows, the growth of LCCO films on *a-axis* oriented YBCO films has resulted in *b-axis* oriented LCCO films. We find this surprising since the growth of LCCO films on *c-axis* oriented YBCO films indicated the same (0 k 0) orientation for the grown LCCO films (Fig. 13c).

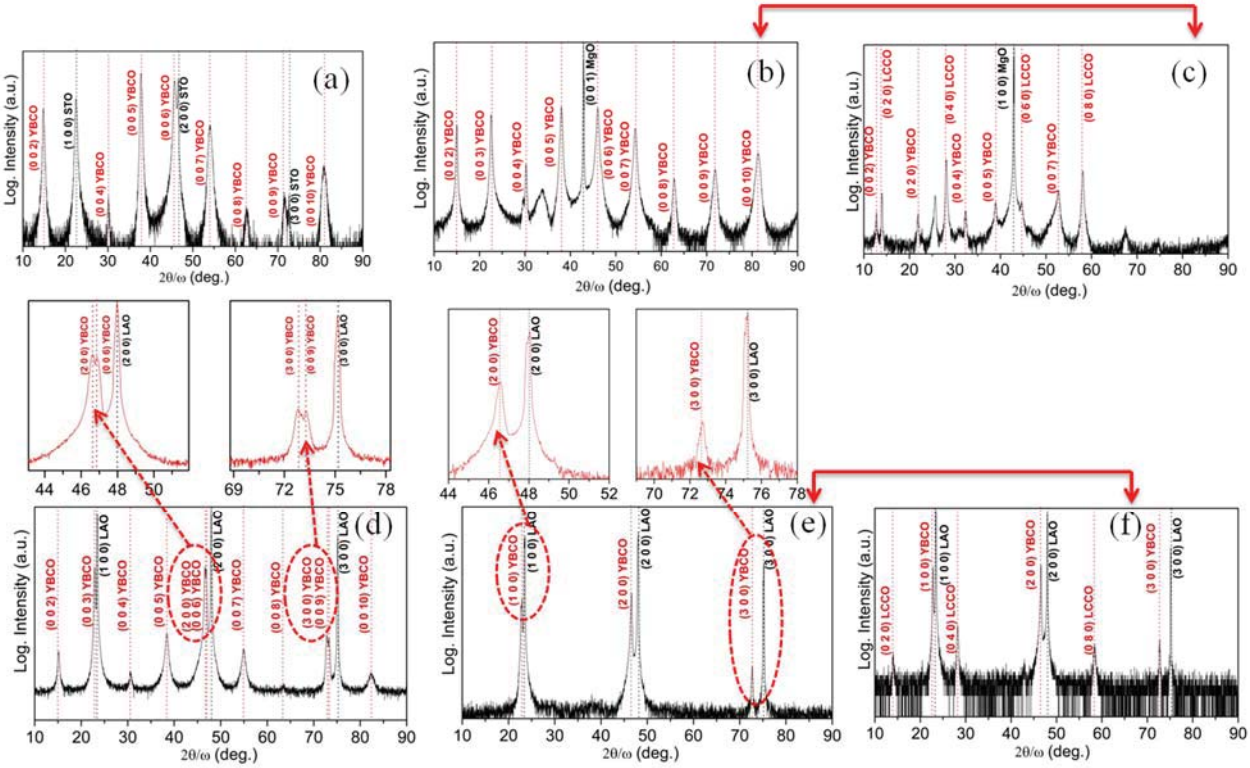

*Figure **13** XRD patterns of: **(a)** a YBCO film grown on (100) STO at 700°C using 250 laser pulses; **(b)** a YBCO film grown on (100) MgO at 700°C using 3500 laser pulses, **(c)** a LCCO film grown on the YBCO film presented in Fig. 12b, **(d)** a YBCO film grown on (100) LAO at 700°C using 250 laser pulses, **(e)** a YBCO film grown on (100) LAO at 630°C using 250 laser pulses; the zoomed figure from above indicates the absence of any (0 0 l) diffraction peaks, and **(f)** a LCCO film grown on the YBCO film presented in Fig. 12e.*

Conclusions

We have succeeded in obtaining epitaxial single-domain *b-axis* LCCO films on (1 1 0) $SrTiO_3$ substrates with bulk-like thermal conductivity values along the cross-plane (*b-axis*) direction (~1 W/m-K). All efforts concerning the growth of epitaxial *c-axis* oriented LCCO films were unsuccessful. Within the elaboration of the project issues such as the growth mode and the response of LCCO films under strain were considered. To this end, we extensively studied the influence of PLD growth parameters: substrate nature, crystallographic orientation, layer thickness and surface termination. Specifically, for Task 1 we deposited LCCO thin films with various thicknesses on (1 0 0), (1 1 0) $SrTiO_3$ and (1 0 0) $SrLaAlO_4$ *flat surface* substrates. We focused on the influence of the strain nature on the domain multiplicity of the grown films. Single-domain LCCO films based on HRXRD and HRTEM studies were obtained on (1 1 0)

$SrTiO_3$ under certain conditions of growth temperature and film thickness. In addition, we investigated the influence of the miscut angle on the films' microstructure in the case of (1 1 0) and (1 0 0) $SrTiO_3$. In all cases the films were surprisingly randomly-oriented. For Task 2, we deposited LCCO films on different substrates either covered with a buffer layer of *a-axis* oriented YBCO or with a high-miscut surface. In all cases, the obtained LCCO films were *b-axis* oriented. It is noted that the *a-axis* oriented YBCO films were grown directly on (1 0 0) LAO substrates. Finally, the proposed third option of using substrates covered with carbon nanotubes was not investigated as we were not able to obtain nanostructures with the desired geometrical dimensions.

Future work

We propose that this project be continued with the objective to resolve the issues which are detrimental to magnon contribution of thermal conductivity in LCCO films. Specifically, we would like to investigate two issues: *stoichiometry* and *layer-by-layer growth mode*, in the case of *b-axis* oriented LCCO films. To this end, we will investigate in depth the effects of all relevant PLD growth conditions (such as laser fluence, repetition rate, substrate temperature, oxygen pressure, etc.) along with those of target composition and film thickness. The latter one is associated with strain effects as discussed in this report. The layer-by-layer growth mode issue will be investigated using an *in-situ* high pressure RHEED system. The goal is to obtain high-thermal-conductivity LCCO films which can be used as *heat spreaders* in nano- and micro-scale devices.

Presentations – Publications

Part of the results discussed in this Final Technical Report were presented in the European – Materials Research Society (E-MRS) Fall Meeting 2015 (Warsaw, Poland) as a contributed poster. The work received the ***Best Poster Award of Symposium V*** (Stress, structure, and stoichiometry effects on the properties of nanomaterials).

In addition part of the results discussed in this Final Technical Report will: (*a*) shortly be submitted for publication in a peer-review journal and (*b*) be included in a chapter titled "*Phase, orientation and morphology control of complex oxide thin films (grown by pulsed laser deposition)*" that we have been invited to contribute by March 31, 2016 for a new book titled

"*Pulsed Laser Ablation: Advances and Applications in Nanoparticles and Nanostructuring Thin Films*", edited by Dr. I. Mihailescu and Dr. Anna Paola Caricato (Pan Stanford Publishing).

Acknowledgements

The HRTEM measurements were carried out in collaboration with Prof. Ch. Lioutas' research group at the Aristotle University of Thessaloniki (Greece). The thermal conductivity TDTR measurements were carried out in collaboration with Prof. D. Cahill's research group at the University of Illinois at Urbana-Champaign (USA).

Methods

All films described in this project have been grown using the Pulsed Laser Deposition (PLD) method employing as ablation source a KrF excimer laser (COMPex Pro 201, λ = 248 nm, τ_{FWHM}= 25 ns). The growth processes were carried out in an ultra-high vacuum (UHV) chamber equipped with a multi-target carousel system. The focused laser beam impinged upon the targets at an angle of 45^0. The targets were set parallel to the substrate and were continuously rotated and toggled in order to ensure a uniform deposition and avoid piercing. Prior to each deposition the chamber was evacuated down to a base pressure less than 5 x 10^{-6} mbar. In order to obtain films with high purity, the targets were pre-ablated before each deposition with ~500 laser pulses. During this procedure, a shutter was interposed between target and substrate to collect the impurities expulsed from the target surface. We reduced the possibility of target decomposition during substrate heating by placing an Al disk between the target and the substrate.*

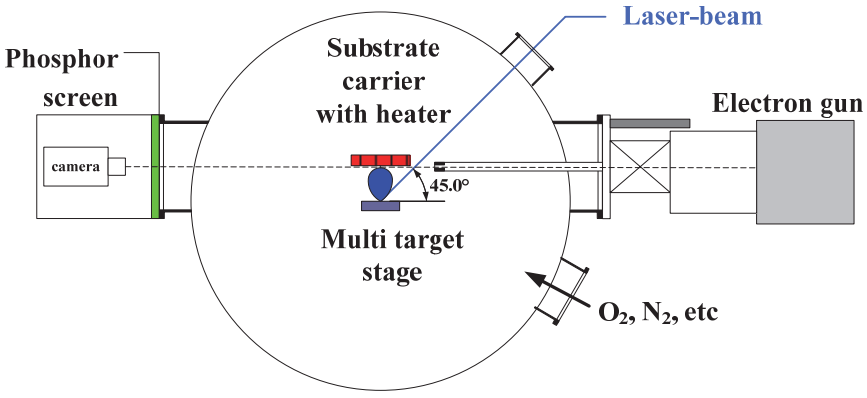

Figure M1 *PLD deposition set-up in Laser-Assisted Materials Processing Laboratory, University of Cyprus.*

The LCCO targets used in the ablation process were prepared by conventional solid state reaction. Powders of La_2O_3, $CaCO_3$ and CuO with purity of 99.99% (Alfa Aesar), were mixed with the molar ratio of La:Ca:Cu = 5:9:24. The obtained powders were then grinded in an agate mortar, and then pressed into pellets with a diameter of 25 mm and a thickness of 5 mm. A sintering process at 900°C for 12h took place in order to ensure the material decarbonization. Finally, the resulting powder was reground and sintered at 950°C for 48h, and again at 970°C for 48h in air, in order to complete the reaction and the crystallization.

Details concerning the crystalline structures were obtained by XRD measurements performed using a Rigaku SmartLab (9kW rotating anode, Cu $K_{\alpha 1}$ radiation,) diffractometer with a parallel beam monochromatized Cu $K_{\alpha 1}$ radiation (measurements accuracy 0.002°) in coplanar measurement geometry. Details concerning the film microstructures were obtained by cross-sectional HRTEM studies using a JEOL 2011 transmission electron microscope working at 200 kV. The samples were prepared by mechanical grinding, followed by ion milling using a GATAN Precision Ion Polishing system.

The films morphology and composition analysis were performed using a Scanning Electron Microscope (SEM) instrument from FEI, model Inspect S, equipped with an EDS unit from EDAX working at an acceleration voltage of up to 30 kV. For our measurements we applied a ZAF (atomic number, absorption and fluorescence correction) standardless quantification with background subtraction matrix correction and normalization to 100%. The results are within 1% margin error, higher for light elements. As a rule, the analysis was conducted at four points for each sample.

The TDTR experiments were performed using a mode-locked Ti:sapphire laser that produces < 0.5 ps pulses at a repetition rate of 80.6 MHz. The measurements were carried out using pump and probe beam powers of 6 and 9 mW, respectively, wavelength λ=700 nm, and a $1/e^2$ beam radius of ~8 μm. Depending on the measurement direction the following experimental parameters have been used: out-of-plane (b-axis direction): 5x objective lens, 9.1 MHz, Ppump = 10 mW, Pprobe = 5 mW; in-plane (a- and c-axis direction) [beam-offset]: 20x objective lens, 1.1MHz (-20ps delay) and 9.1MHz (+50ps), Ppump = 2mW, Pprobe = 1 mW. For out-of-plane measurement, the error bar was calculated based on the calculation of sensitivity and uncertainty of each input parameter using the following equation:

$$U_\lambda = \sqrt{\sum_\alpha \frac{S\alpha}{S\lambda} * U\lambda}$$

where:

$U\lambda$ = the uncertainty of the thermal conductivity of sample

$U\alpha$ = the uncertainty of the input parameter

$S\lambda$ = the sensitivity to the thermal conductivity of sample

$S\alpha$ = the sensitivity to the input parameter.

For the in-plane measurement, the error bar was calculated based on the uncertainty of the thermal conductivity of NbV (the metal coating). The parameters used in analyzing the TDTR data:

	NbV	*LCCO*	*(1 1 0) STO*
λ (W/m · K)	*19.5 ± 1*	*To be measured*	*11.2*
Cp ($J/m^3 \cdot K$)	*$2.65 \cdot 10^6$*	*$2.89 \cdot 10^6$ (Debye limit)*	*$2.79 \cdot 10^6$*